RSC Advances

PAPER

View Article Online
View Journal | View Issue

Cite this: *RSC Adv.*, 2020, **10**, 3539

Zinc-tetracarboxylate framework material with nano-cages and one-dimensional channels for excellent selective and effective adsorption of methyl blue dye†

Qipeng Li,[ab] Jinjie Qian,[*c] Lin Du*[a] and Qihua Zhao[*a]

Received 31st October 2019
Accepted 14th January 2020

DOI: 10.1039/c9ra08983g

rsc.li/rsc-advances

An example of a zinc-tetracarboxylate framework material (**FJI-11**) was solvothermally synthesized and structurally characterized. **FJI-11** presented 3D cage-stacking frameworks with octahedral cages, cuboctahedral cages and two kinds of 1D channel along the *c*-axis. In addition, **FJI-11** exhibited the excellent selective and effective adsorption of methyl blue (MB) dye by guest molecule exchange, and its adsorption process was in accordance with the second-order kinetic model and the Freundlich model.

Introduction

Organic dye wastewater comes from the cosmetic, textile, paper and pharmaceutical industries, and has become one of the most serious environmental pollutants due to being highly toxic and difficult to degrade; its release into the aquatic ecosystem can destroy the ecological environment.[1,2] As one of the stable organic dye molecules, methyl blue (MB) is toxic and might cause the unwanted effects of nausea, abdominal pain, dizziness, headache, sweating and confusion.[3] Currently, many methods have been employed for the treatment of MB wastewater, such as the degradation method, coagulation method, oxidation method, filtration method, adsorption method, radiation method and biological method, but each method has different advantages and disadvantages.[1a,4] The adsorption method with the advantages of simplicity, convenience, high efficiency and obvious adsorption effect, has been considered as a very effective and proven technology for the removal of MB dye.[5] Many adsorption materials including activated carbon, zeolites, molecular sieves and metal organic frameworks (MOFs) have been reported, while the search for and development of adsorption materials for the selective and effective adsorption of MB dye is of great significance and also a challenge.[6]

MOFs often have multifarious intriguing topologies and fascinating structures, which have the potential application as functional materials in the fields of fluorescence, magnetic, gas storage, catalysis, organic dye adsorption and so forth.[7,8] Compared with the zeolite, molecular sieve and activated carbon, MOFs have the advantages of adjustable frame structure, high porosity, large specific surface area and simple synthesis process.[9] To date, some MOFs have been used for the removal or degradation of MB dye, while the MOFs with the excellently selective and effective adsorption capacity have been rarely investigated.[10,11] However, the design and construction of more MOFs with the excellently selective and effective adsorption of MB dye are desperately required.

Hence, we prepared an example of zinc-tetracarboxylate framework, formulated as $[Zn_2(bptc)(H_2O)_2]\cdot 5DMA$ (**FJI-11**, H_4bptc = biphenyl-3,3′,5,5′-tetracarboxylic acid), which displayed the 3D cage-stacking frameworks with octahedral cages, cuboctahedral cages and two kinds of 1D channels along the *c*-axis. In addition, **FJI-11** exhibited the excellently selective and effective adsorption of MB dye and its adsorption process was in accordance with the second-order kinetic model and Freundlich model.

Results and discussion

Synthesis and structure description

Cubic shaped crystals of **FJI-11** are obtained by the solvothermal reaction of $Zn(NO_3)_2\cdot 6H_2O$ and H_4bptc in the mixed-solvent of DMA and 1,4-dioxane (1 : 1, v/v) with the addition of 0.2 mL nitric acid (65 wt%) at 85 °C for 5 days. The phase purity of the as-synthesized product of **FJI-11** was confirmed by the powder X-ray diffraction analysis (XRD). The final molecular formula of

[a]*Key Laboratory of Medicinal Chemistry for Natural Resource Education Ministry, School of Chemical Science and Technology, Yunnan University, Kunming, 650091, P. R. China. E-mail: lindu@ynu.edu.cn; qhzhao@ynu.edu.cn*

[b]*Science and Technology Department, College of Chemistry and Chemical Engineering, Zhaotong University, Zhaotong, 657000, P. R. China*

[c]*College of Chemistry and Materials Engineering, Wenzhou University, Wenzhou, 325035, P. R. China. E-mail: jinjieqian@wzu.edu.cn*

† Electronic supplementary information (ESI) available: Crystal data, TGA, PXRD patterns, UV data, luminescent spectra and other materials for **FJI-11**. CCDC 1909611. For ESI and crystallographic data in CIF or other electronic format see DOI: 10.1039/c9ra08983g

FJI-11 was calculated from the SQUEEZE results combined with the thermogravimetric analysis (TGA) data and elemental analysis (EA) data.

Single crystal X-ray diffraction analysis indicates that **FJI-11** is crystallized in the trigonal space group $R\bar{3}m$ with the lattice parameters $a = b = 18.7428(8)$ Å, $c = 24.915(2)$ Å, $\alpha = \beta = 90°$ and $\gamma = 120°$, and its asymmetry unit consists of one half of independent Zn(II) ion, a quarter of $bptc^{4-}$ ligand and one half of terminally coordinated water molecule (Fig. S1†). The central Zn(II) ions are five-coordinated by four carboxylate O atoms from four different $bptc^{4-}$ ligands and one half O atom from the coordinated water. The $bptc^{4-}$ ligand displays a $(\kappa^1\text{-}\kappa^1)\text{-}(\kappa^1\text{-}\kappa^1)\text{-}(\kappa^1\text{-}\kappa^1)\text{-}(\kappa^1\text{-}\kappa^1)\text{-}\mu_8$ coordination mode and two Zn(II) ions are linked by four bridging carboxylate generate the $Zn_2(COO)_4$ paddle wheel SBUs (Fig. S2†). **FJI-11** is analogue of MOF-505, MOF-505 series and NOTT-100 series, which consists of two different types of alternative packed open cages.[12] Every twelve $bptc^{4-}$ ligands connects six $Zn_2(COO)_4$ paddle wheel SBUs, to generate a octahedral cage with the diameter of about 9 Å (Fig. 1a), then eight octahedral assembled into a cuboctahedral cage with the elliptical cavity is about 14×8 Å^2 (Fig. 1b). Two different types of cages are connected to each other by sharing the triangular and quadrangular windows and arranging in an alternating fashion,[12] forming a 3D cage-stacking framework with two kinds of 1D channels (the diameter of about 7.5 Å) along the *c*-axis (Fig. 1c and Fig. S3†).

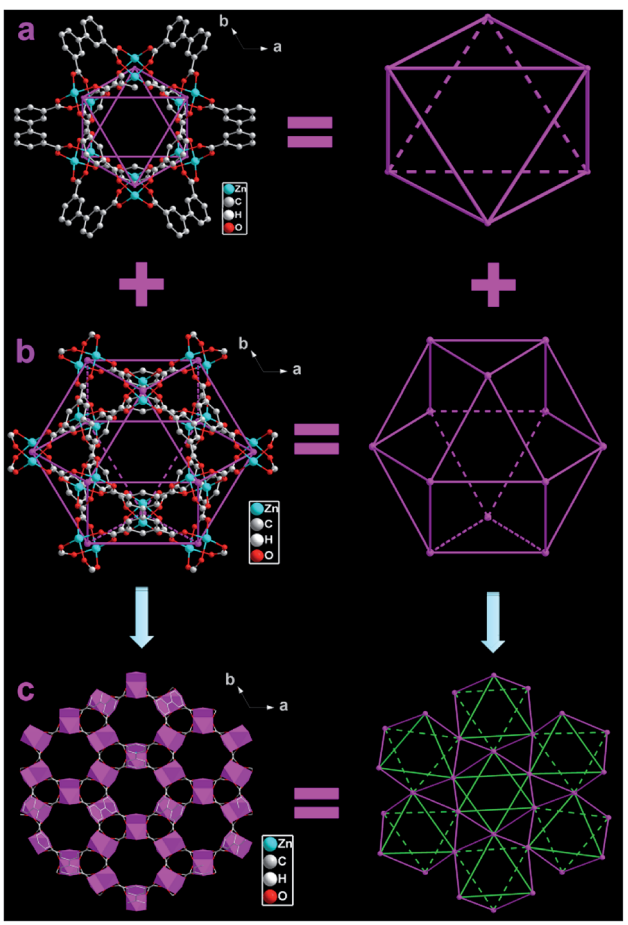

Fig. 1 (a) The octahedral cage composed of $Zn_2(CO_2)_4$ paddle wheel SBUs and $bptc^{4-}$ ligands. (b) The cuboctahedral cage constructed by eight octahedral cages. (c) The 3D cage-stacking framework in **FJI-11**.

Luminescence property

The solid state luminescence properties of **FJI-11** and the free H_4bptc ligand were explored at room temperature. The free H_4bptc ligand exhibited an emission with the peaking at 372 nm (λ_{ex} = 321 nm), while **FJI-11** displayed a maximum emission at 439 nm (λ_{ex} = 341 nm) (Fig. 2 and S6†). The maximum emission peak of **FJI-11** exhibited the red shift phenomenon compared with that of the free H_4bptc ligand. In addition, the luminescence mechanism of **FJI-11** might be assigned to the π–π* fluorescent emissions of $bptc^{4-}$ ligand to Zn(II) charge transition (LMCT).[13]

Sorption behaviour

The total volume of cavity in **FJI-11** with the removal of the disordered guest solvent molecules and coordinated water molecules was calculated by the PLATON Program,[14] which is approximately 61.5% (solvent area volume 4659.4 Å^3 and unit cell volume 7579.90 Å^3). In order to characterize the porosity of **FJI-11**, the crystal samples of **FJI-11** were activated by the supercritical carbon dioxide (SCD) method and the N_2 adsorption–desorption isotherms of activated **FJI-11** sample was performed at 77 K. **FJI-11** exhibited the pseudo-type I nitrogen isotherm with the saturated N_2 capacity of 299.8 cm^3 g^{-1} at 77 K (Fig. 3), and the corresponding to Brunauer–Emmett–Teller (BET) and Langmuir surface areas of 1121.01 m^2 g^{-1} and 1283.88 m^2 g^{-1}.[15] Meanwhile, the DFT pore size distribution (PSD) analysis reveals that the percentage of microspores centered at 6–8 Å and the maximum distribution centered approximately at 7.25 Å (Fig. 3), which accords well with the internal structural features of nano-cages and one-dimensional channels.

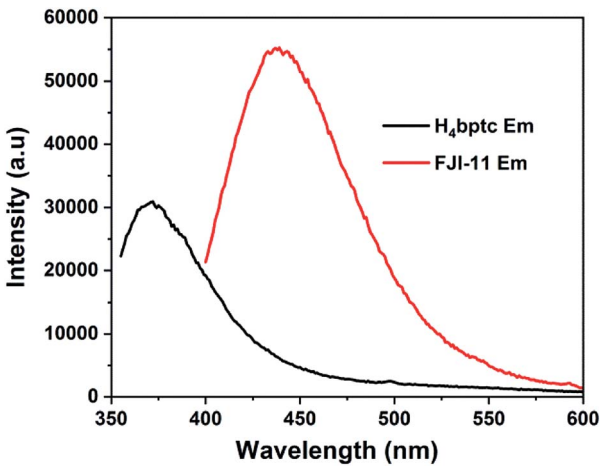

Fig. 2 Solid state emission spectra of the free H_4bptc ligand and **FJI-11**.

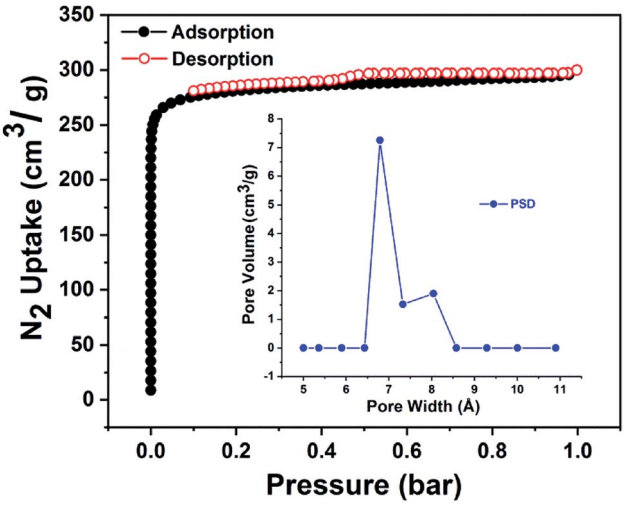

Fig. 3 Experimental nitrogen adsorption–desorption isotherms at 77 K for FJI-11; inset shows the pore size distribution (PSD) calculated by the DFT method.

Adsorption capability of FJI-11 towards organic dye

In order to investigate the dye adsorption behaviors in **FJI-11**, the methylene blue (MB), methyl orange (MO), rhodamine B (RB) and rhodamine 6G (R6G) with different sizes and configurations were chosen for the adsorption experiments (Fig. S7†). The prepared crystalline sample (10 mg) of **FJI-11** was immersed in the dye-containing acetonitrile solution (10 mg L^{-1}), to evaluate its adsorption abilities by the guest molecule exchange, and the concentrations of the organic dyes before and after the adsorption experiments were menstruated by the UV/Vis spectrophotometer. As shown in Fig. 4, the color of the MB solution obviously changed from blue to the colorless, but the colors of the MO, RB and R6G solutions were no significant change, which were consistent with the UV-Vis spectroscopy results. These results indicated that **FJI-11** could exhibit the excellently selective and effective adsorption of MB dye (Table S2†).[16]

In order to investigate the MB adsorption process in **FJI-11**, the kinetic adsorption and thermodynamics adsorption experiment were carried out. The kinetic adsorption experiment was investigated by the initial MB concentration of 10 mg L^{-1} under different concussion times, the experiment data was well fitted by the pseudo-second-order kinetic model[17,18] (Fig. 5a). In addition, the thermodynamics adsorption experiment was investigated under different initial MB concentration at 25 °C, the experiment data was well fitted by the Freundlich model[17,18] (Fig. 5b).

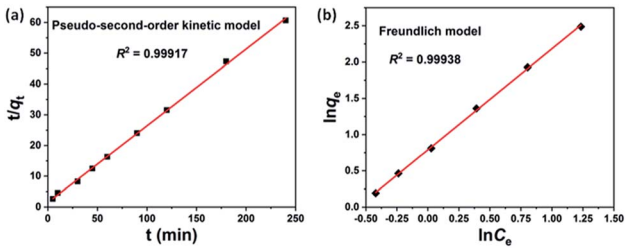

Fig. 5 (a) Pseudo-second-order kinetic model of MB adsorption in FJI-11. (b) Freundlich model of MB adsorption in FJI-11.

These results suggest that the proposed adsorption mechanism of MB in **FJI-11** was a chemical process, which occurred into the nano-cages and one-dimensional channels by the hydrogen bonding interaction and guest molecule exchange in **FJI-11**.[18] Due to the cavity size effect (the maximum pore size distribution centered about at 7.25 Å in **FJI-11**, but the molecular sizes of RB and R6G were more than 7.25 Å) and the hydrogen bonding interaction (the N atom from the MB and the coordinated water molecules from **FJI-11**), **FJI-11** only exhibited the excellently selective and effective adsorption of MB dye.[17,18]

Experimental

Materials and physical measurements

Reactions were carried out in 20 mL glass vials under autogenous pressure. All the reactants are of reagent-grade quality and used as purchased commercially without further purification. The power X-ray diffraction patterns (XRD) were collected by a Rigaku D using Cu Kα radiation (λ = 0.154 nm). Elemental analyses for C, H, N were carried out on a German Elementary Vario EL III instrument. Thermogravimetric analyses (TGA) were recorded on a NETZSCH STA 449C unit at a heating rate of 10 °C min^{-1} under flowing nitrogen atmosphere. Fluorescence spectra of the solid samples were performed on an Edinburgh Analytical instrument FLS920. Single gas adsorption measurements were performed in the Accelerated Surface Area and Porosimetry 2020 (ASAP2020). UV-Vis absorption spectra were recorded on a Purkinje General Instrument T6 new century.

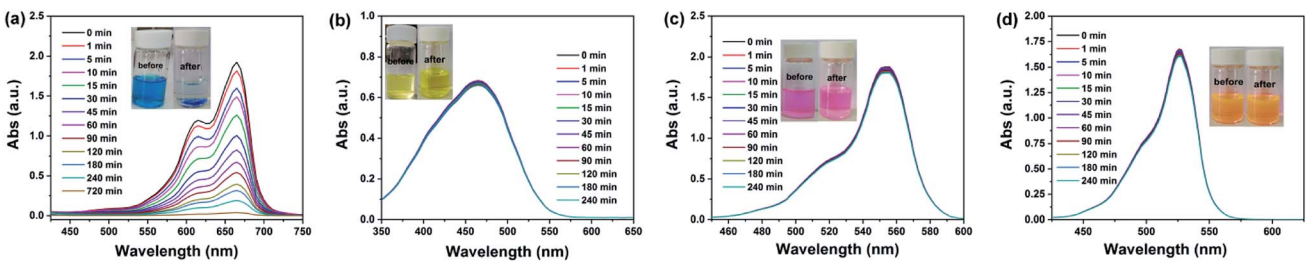

Fig. 4 The adsorption experiments of (a) methylene blue (MB), (b) methyl orange (MO), (c) rhodamine B (RB) and (d) rhodamine 6G (R6G) in FJI-11.

Table 1 The crystal data and structure refinement for FJI-11

Compounds	**FJI-11**
CCDC	1909611
Formula	$C_{46}H_{55}N_{10}O_{15}Zn_2$
M_r	1118.76
Space group	$R\bar{3}m$
a (Å)	18.7428(8)
b (Å)	18.7428(8)
c (Å)	24.915(2)
α (deg.)	90
β (deg.)	90
γ (deg.)	120
V (Å^3)	7579.9(10)
Z	9
D_c (g cm^{-3})	2.206
M (mm^{-1})	1.481
F(000)	3429.0
GOF	1.062
R_1[a]	0.0352
wR_2[a]	0.0878

[a] $R = \sum(||F_o| - |F_c||)/\sum|F_o|$, $wR = \{\sum w[(F_o^2 - F_c^2)^2]/\sum w[(F_o^2)^2]\}^{1/2}$; [$F_o > 4$ (F_o)].

Synthesis of $[Zn_2(bptc)(H_2O)_2]\cdot 5DMA$ (FJI-11)

A mixture of $Zn(NO_3)_3\cdot 6H_2O$ (0.40 mmol, 120 mg) and H_4bptc (0.1 mmol, 33 mg), in *N*,*N*-dimethylacetamide (DMA) (3.0 mL) and 1,4-dioxane (3.0 mL) with an additional HNO_3 (0.2 mL, 65 wt%) was sealed in a 20 mL glass vial, which was heated at 85 °C for 5 days, and cooled down to room temperature. After washing with fresh DMA, the crystals were obtained in *ca.* 58% yield based on the $Zn(NO_3)_3\cdot 6H_2O$. Elemental analysis was calculated for **FJI-11**: C, 49.38%; H, 4.96%; N, 12.52%. Found: C, 49.12%; H, 4.93%; N, 12.55%.

Single-crystal X-ray crystallography

The structures data of **FJI-11** was collected on a Rigaku Mercury CCD diffract meter equipped with a graphite-monochromated Mo Kα radiation (λ = 0.71073 Å) at room temperature and the structure was resolved by the direct method and refined by full-matrix least-squares fitting on F^2 by Olex2 program.[19] We employed the PLATON/SQUEEZE to calculate the contribution to the diffraction from the solvent region and thereby produced a set of solvent-free diffraction intensities.[20] The final formula of **FJI-11** was calculated from the SQUEEZE results combined with elemental analysis data and TGA data. More details on the crystallographic studies as well as atomic displacement parameters are given in ESI† as CIF files. Crystallographic data for the structures reported in this paper have been deposited. The following crystal structure has been deposited at the Cambridge Crystallographic Data Centre and allocated the deposition number CCDC: 1909611 for **FJI-11**. Crystallographic data and structure refinement parameters for **FJI-11** are summarized in Table 1 and the selected bond lengths and angles of **FJI-11** are listed in Table S1.†

Conclusions

In summary, an example of zinc-tetracarboxylate framework material (**FJI-11**) has been successfully synthesized and structurally characterized. The 3D cage-stacking framework of **FJI-11** was constructed by the octahedral cages, cuboctahedral cages and two kinds of 1D channel along the *c*-axis. **FJI-11** exhibited the excellently selective and effective adsorption of MB dye by the guest molecule exchange, and its adsorption process was in accordance with second-order kinetic model and Freundlich model. Our results are helpful for the preparation of more porous MOFs with the excellently selective and effective adsorption of the organic dyes in the future.

Conflicts of interest

There are no conflicts to declare.

Acknowledgements

This work was supported by the National Natural Science Foundation of China (21861044 and 21561033), the Project funded by China Postdoctoral Science Foundation (2018M633426) and the Project funded by Yunnan Province Postdoctoral Science Foundation (2018).

Notes and references

1 (*a*) C. C. Wang, J. Li, X. L. Lv, Y. Q. Zhang and G. S. Guo, *Energy Environ. Sci.*, 2014, **7**, 2831–2867; (*b*) Y. Shen, Q. Fang and B. Chen, *Environ. Sci. Technol.*, 2015, **49**, 67–84; (*c*) Q. Gao, J. Xu and X. H. Bu, *Coord. Chem. Rev.*, 2019, **378**, 17–31.

2 (*a*) I. Ali, M. Asim and T. A. Khan, *J. Environ. Manage.*, 2012, **113**, 170–183; (*b*) G. Liu, X. Li, J. Zhao, H. Hidaka and N. Serpone, *Environ. Sci. Technol.*, 2000, **34**, 3982–3990; (*c*) C. C. Jin, D. M. Liu, J. Hu, Y. Wang, Q. Zhang, L. Lv and F. W. Zhuge, *Nano Energy*, 2019, **59**, 372–379.

3 (*a*) C. Jack and L. Jerrold B, *Am. J. Therapeut.*, 2003, **10**, 289–291; (*b*) M. Rafatullah, O. Sulaiman, R. Hashima and A. Ahmad, *J. Hazard. Mater.*, 2010, **177**, 70–80.

4 (*a*) M. B. Ahmed, J. L. Zhou, H. H. Ngo, W. S. Guo, N. S. Thomaidis and J. Xu, *J. Hazard. Mater.*, 2017, **323**, 274–298; (*b*) P. M. Pakdel and S. J. Peighambardoust, *Carbohydr. Polym.*, 2018, **201**, 264–279; (*c*) Y. J. Yao, F. F. Xu, M. Chen, Z. X. Xu and Z. W. Zhu, *Bioresour. Technol.*, 2010, **101**, 3040–3046; (*d*) R. Wo, Q. L. Li, C. Zhu, Y. Zhang, G. F. Qiao, K. Y. Lei, P. Du and W. Jiang, *J. Chem. Eng. Data*, 2019, **64**, 2455–2463.

5 (*a*) S. W. Lv, J. M. Liu, H. Ma, Z. H. Wang, C. Y. Li, N. Zhao and S. Wang, *Microporous Mesoporous Mater.*, 2019, **282**, 179–187; (*b*) Y. Ren, T. Li, W. M. Zhang, S. Wang, M. Q. Shi, C. Shan, W. B. Zhang, X. H. Guan, L. Lv, M. Hua and B. C. Pan, *J. Hazard. Mater.*, 2019, **365**, 312–321.

6 (*a*) Y. Xu, J. Jin, X. Li, Y. Han, H. Meng, T. Wang and X. Zhang, *RSC Adv.*, 2015, **5**, 19199–19202; (*b*) S. Lin, Z. Song, G. Che, A. Ren, P. Li, C. Liu and J. Zhang, *Microporous Mesoporous Mater.*, 2014, **193**, 27–34; (*c*) S. L. Xiao, Y. H. Li, P. J. Ma and G. H. Cui, *Inorg. Chem. Commun.*, 2013, **37**, 54–58; (*d*) R. Ahmad and R. Kumar, *Appl. Surf. Sci.*, 2010, **257**, 1628–1633; (*e*) M. Bhaumik,

R. McCrindle and A. Maity, *Chem. Eng. J.*, 2013, **228**, 506–515; (*f*) W. Cai, Y. Hu, J. Chen, G. Zhang and T. Xia, *CrystEngComm*, 2012, **14**, 972–977; (*g*) W. Yan, L. J. Han, H. L. Jia, K. Shen, T. Wang and H. G. Zheng, *Inorg. Chem.*, 2016, **55**, 8816–8821; (*h*) X. Wang, Z. J. Ma, L. L. Chai, L. Q. Xu, Z. Y. Zhu, Y. Hu, J. J. Qian and S. M. Huang, *Carbon*, 2019, **141**, 643–651; (*i*) X. Wang, L. L. Chai, J. Y. Ding, L. Zhong, Y. J. Du, T. T. Li, Y. Hu, J. J. Qian and S. M. Huang, *Nano Energy*, 2019, **62**, 745–753.

7 (*a*) G. Maurin, C. Serre, A. Cooper and G. Férey, *Chem. Soc. Rev.*, 2017, **46**, 3104–3107; (*b*) N. S. Bobbitt, M. L. Mendonca, A. J. Howarth, T. Islamoglu, J. T. Hupp, O. K. Farha and R. Q. Snurr, *Chem. Soc. Rev.*, 2017, **46**, 3357–3385.

8 (*a*) C. H. Wang, X. L. Liu, N. K. Demir, J. P. Chen and K. Li, *Chem. Soc. Rev.*, 2016, **45**, 5107–5134; (*b*) Y. Bai, Y. B. Dou, L. H. Xie, J. R. Li and H. C. Zhou, *Chem. Soc. Rev.*, 2016, **45**, 2327–2367.

9 (*a*) G. M. Espallargas and E. Coronado, *Chem. Soc. Rev.*, 2018, **47**, 533–557; (*b*) M. O. Keeffe and O. M. Yaghi, *Chem. Rev.*, 2012, **112**, 675–702; (*c*) M. Li, D. Li, M. O. Keeffe and O. M. Yaghi, *Chem. Rev.*, 2014, **114**, 1343–1370.

10 (*a*) P. P. Yu, Q. P. Li, Y. Hu, N. N. Liu, L. J. Zhang, K. Z. Su, J. J. Qian, S. M. Huang and M. C. Hong, *Chem. Commun.*, 2016, **52**, 7978–7981; (*b*) Y. Y. Cui, J. Zhang, L. L. Ren, A. L. Cheng and E. Q. Gao, *Polyhedron*, 2019, **161**, 71–77; (*c*) C. Li, Z. h. Xiong, J. M. Zhang and C. S. Wu, *J. Chem. Eng. Data*, 2015, **60**, 3414–3422; (*d*) J. H. Qiu, Y. Feng, X. F. Zhang, M. M. Jia and J. F. Yao, *J. Colloid Interface Sci.*, 2017, **499**, 151–158; (*e*) M. L. Gao, W. J. Wang, L. Liu, Z. B. Han, N. Wei, X. M. Cao and D. Q. Yuan, *Inorg. Chem.*, 2017, **56**, 511–517.

11 (*a*) M. Z. Wu, J. Y. Shi, P. Y. Chen, L. Tian and J. Chen, *Inorg. Chem.*, 2019, **58**, 3130–3136; (*b*) X. J. Gao, G. H. Sun, F. Y. Ge and H. G. Zheng, *Inorg. Chem.*, 2019, **58**, 8396–8407; (*c*) Y. Li, F. T. Liu, H. X. Zhang, X. Li, X. F. Dong and C. W. Wang, *Appl. Surf. Sci.*, 2019, **484**, 144–151.

12 (*a*) Y. Wang, H. F. Cao, B. S. Zheng, R. F. Zhou and J. G. Duan, *Cryst. Growth Des.*, 2018, **18**, 7674–7682; (*b*) Q. P. Li, J. G. Luo, L. Wang, C. Qi, Y. S. Yang, X. J. Zhang and J. J. Qian, *CrystEngComm*, 2017, **19**, 214–217; (*c*) B. L. Chen, N. W. Ockwig, A. R. Millward, D. S. Contreras and O. M. Yaghi, *Angew. Chem., Int. Ed.*, 2005, **44**(30), 4745–4749; (*d*) Y. X. Hu, S. C. Xiang, W. W. Zhang, Z. X. Zhang, L. Wang, J. F. Bai and B. L. Chen, *Chem. Commun.*, 2009, **48**, 7551–7553; (*e*) Y. Yan, S. H. Yang, A. J. Blake and M. Schroder, *Acc. Chem. Res.*, 2014, **47**(2), 296–307.

13 (*a*) W. P. Lustig, S. Mukherjee, N. D. Rudd, A. V. Desai, J. Li and S. K. Ghosh, *Chem. Soc. Rev.*, 2017, **46**, 3242–3285; (*b*) Q. P. Li, Z. Y. Zhu and J. J. Qian, *Polyhedron*, 2018, **155**, 218–222; (*c*) Q. P. Li and J. J. Qian, *RSC Adv.*, 2014, **4**, 32391–32397; (*d*) L. Chen, C. Yan, M. Pan, H. P. Wang, Y. N. Fan and C. Y. Su, *Eur. J. Inorg. Chem.*, 2016, **17**, 2676–2680.

14 (*a*) A. L. Spek, *PLATON, A Multipurpose Crystallographic Tool*, Utrecht University, 2001; (*b*) J. G. Duan, Z. Yang, J. F. Bai, B. S. Zheng, Y. Z. Li and S. H. Li, *Chem. Commun.*, 2012, **48**, 3058–3060.

15 (*a*) Y. J. Du, L. Zhong, Y. Hu, Q. P. Li and J. J. Qian, *CrystEngComm*, 2019, **21**, 5045–5049; (*b*) J. J. Qian, Q. P. Li, L. F. Liang, T. T. Li, Y. Hu and S. M. Huang, *Dalton Trans.*, 2017, **46**, 14102–14106; (*c*) S. H. Yang, J. L. Sun, A. J. Ramirez-Cuesta, S. K. Callear, W. I. F. David, D. P. Anderson, R. New by, A. J. Blake, J. E. Parker, C. C. Tang and M. Schröder, *Nat. Chem.*, 2012, **4**, 887–894; (*d*) M. Savage, I. Silva, M. Johnson, J. H. Carter, R. Newby, M. Suyetin, E. Besley, P. Manuel, S. Rudić, A. N. Fitch, C. Murray, W. I. F. David, S. H. Yang and M. Schröder, *J. Am. Chem. Soc.*, 2016, **138**, 9119–9127.

16 (*a*) M. Hasanzadeh, A. Simchi and H. S. Far, *J. Ind. Eng. Chem.*, 2020, **81**, 405–414; (*b*) M. Hasanzadeh, A. Simchi and H. S. Far, *Mater. Chem. Phys.*, 2019, **233**, 267–275; (*c*) M. Pęgier, K. Kilian and K. Pyrzynska, *Monatshefte Chem.*, 2019, **150**, 1569–1572; (*d*) L. Zhang, J. S. Sun, F. X. Sun, P. Chen, J. Liu and G. S. Zhu, *Chem.–Eur. J.*, 2019, **25**, 3903–3908.

17 (*a*) P. Huang, C. Chen, M. Wu, F. Jiang and M. Hong, *Dalton Trans.*, 2019, **48**, 5527–5533; (*b*) M. Mon, R. Bruno, J. F. Soria, D. Armentano and E. Pardo, *J. Mater. Chem. A*, 2018, **6**, 4912–4947; (*c*) F. L. Hu, Z. Y. Di, P. Lin, P. Huang, M. Y. Wu, F. L. Jiang and M. C. Hong, *Cryst. Growth Des.*, 2018, **18**, 576–580; (*d*) K. Z. Su, W. J. Wang, B. B. Li and D. Q. Yuan, *ACS Sustainable Chem. Eng.*, 2018, **6**, 17402–17409; (*e*) M. Zhou, Z. F. Ju and D. Q. Yuan, *Chem. Commun.*, 2018, **54**, 2998–3001.

18 (*a*) L. N. Jin, X. Y. Qian, J. G. Wang, H. Aslan and M. Dong, *J. Colloid Interface Sci.*, 2015, **453**, 270–275; (*b*) J. M. Yang, R. J. Ying, C. X. Han, Q. T. Hu, H. M. Xu, J. H. Li, Q. Wang and W. Zhang, *Dalton Trans.*, 2018, **47**, 3913–3920; (*c*) S. Lin, Z. Song, G. Che, A. Ren, P. Li, C. Liu and J. Zhang, *Microporous Mesoporous Mater.*, 2014, **193**, 27–34; (*d*) L. Xiao, Y. Xiong, Z. Wen and S. Tian, *RSC Adv.*, 2015, **5**, 61593–61600; (*e*) P. Z. Li, X. J. Wang, S. Tan, C. Ang, H. Chen, J. Liu, R. Zou and Y. Zhao, *Angew. Chem., Int. Ed.*, 2015, **54**, 12748–12752; (*f*) J. Ai, H. R. Tian, X. Min, Z. C. Wang and Z. M. Sun, *Dalton Trans.*, 2020, DOI: 10.1039/c9dt01545k.

19 (*a*) G. M. Sheldrick, SHELXS, *Acta Crystallogr.*, 2008, **A64**, 112–122; (*b*) M. Sheldrick, *Acta Crystallogr.*, 2015, **C71**, 3–8.

20 (*a*) A. L. Spek, *J. Appl. Crystallogr.*, 2003, **36**, 7; (*b*) P. v. d. Sluis and A. L. Spek, *Acta Crystallogr., Sect. A: Found. Crystallogr.*, 1990, **46**, 194; (*c*) A. L. Spek, *Acta Crystallogr.*, 2015, **C71**, 9; (*d*) Q. P. Li, Z. Y. Zhu and J. J. Qian, *Polyhedron*, 2018, **155**, 218–222; (*e*) Q. P. Li, Y. Peng, J. J. Qian, T. Yan, L. Du and Q. H. Zhao, *Dalton Trans.*, 2019, **48**, 12880–12887.